


Effect of FRP strengthening on the flexural behaviour of calcarenite masonry walls

Giovanni Minafò¹  · Calogero Cucchiara¹ · Alessia Monaco¹ · Lidia La Mendola¹

Received: 25 February 2016 / Accepted: 27 February 2017 / Published online: 4 March 2017
© Springer Science+Business Media Dordrecht 2017

Abstract The use of fiber-reinforced polymers (FRP) for structural strengthening has become increasingly popular in recent years. Several applications of FRP have been proposed and applied, depending on the target of the technique, kind and/or material of the structural member. In particular, because of their great tensile strength, FRP materials are commonly used to enhance the out-of-plane behaviour of masonry walls, allowing to increase their strength, ductility and improving safety against overturning. For these reasons, FRP laminates are often applied in vulnerable ancient buildings in seismic areas to reinforce façades and walls with poor structural features. However, some issues arise when adopting composites in historical constructions, the most related to the aesthetical impact of laminates and compatibility between FRP and masonry. Consequently, a correct evaluation of the reinforcement percentages for strength and ductility purposes is crucial, as well as the effective increase of structural performances. This paper presents a numerical-analytical approach able to reproduce the flexural behaviour of out-of-plane loaded masonry walls. The model is based on a simplified representation of the member, the latter modeled as a cantilever beam. Mechanical non-linearity is introduced by means of moment–curvature relationships, deduced with proper constitutive laws of masonry and by taking into account the ultimate debonding strain of FRP. Second order effects are considered by adopting an iterative step-by-step procedure. Comparisons are made in terms of moment–curvature and load–displacement curves with experimental data available in the literature and with non-linear finite element analyses, showing both good agreement. Finally, parametric considerations on the reinforcement percentages are made in terms of strength and ductility.

Keywords Masonry walls · FRP strengthening · Out-of-plane loading

✉ Giovanni Minafò
giovanni.minafò@unipa.it

¹ Dipartimento di Ingegneria Civile, Ambientale, Aerospaziale, dei Materiali (DICAM), Viale delle Scienze, 90128 Palermo, Italy

1 Introduction

The preservation of the built environment and heritage represents a very topical subject for the scientific community all over the world. Several studies in the literature are addressed to the development of effective procedures for the assessment and mitigation of the seismic risk, modeling of masonry buildings in old urban centers or also the set-up of nonlinear static and dynamic analyses able to take into account the real behavior of materials.

Particularly, in the last decades, the interest toward the restoration of ancient masonry buildings and historic structures is increasing with particular regard to the use of innovative materials and techniques for enhancing the structural performances under both normal and severe load conditions. To this scope, fiber-reinforced polymers (FRP) are increasingly in use for the structural strengthening as well as for improving ductility and safety against overturning failure mechanism. Several applications have been proposed and applied and specific prescriptions are contained within the reference codes.

The main advantages in the use of FRP are high mechanical properties, contained weight and thickness, absence of corrosion, easy installation with the possibility of maintaining the serviceability of the structure during the process, reversibility of the intervention. Actually, also a series of disadvantages should be mentioned, such as high costs, reduced heat resistance and elastic-fragile behaviour of the material.

The increasingly large use of FRP led to the development of specific guidelines for the design procedures: CNR-DT 200 R1/2013 represents the reference Italian code, while ACI Committee 440 (2010) and ISIS Design Manual No. 4 (2008) are the American and Canadian ones. Finally, FIB Bulletin (2001, 2007) represents the international reference guideline.

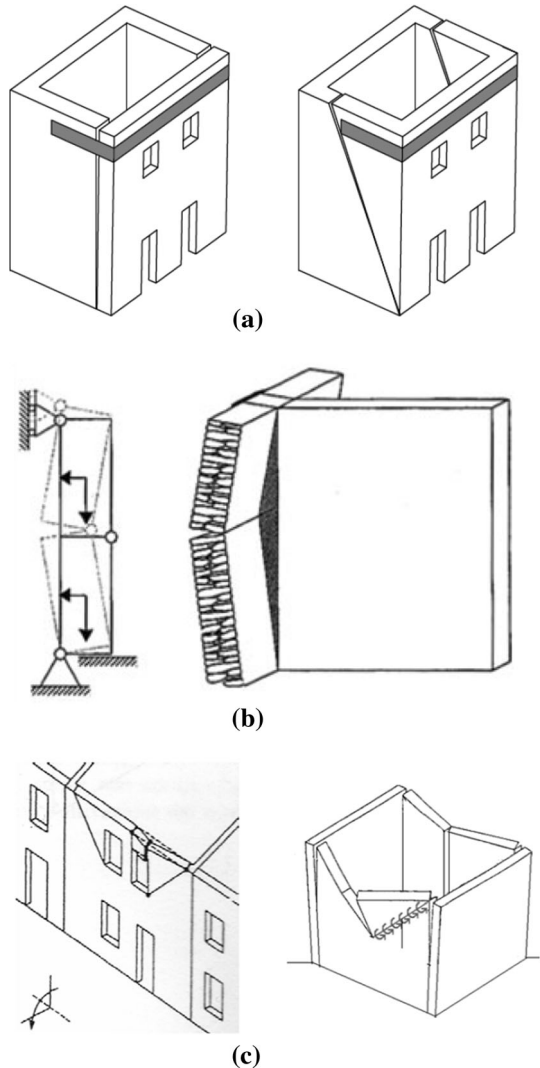
Particularly, with regard to masonry, prescriptions are provided on the verification of the flexural behaviour of out-of-plane loaded walls, which is one of the most common local failure mechanism generally occurring in such elements. The mechanism can be attributed to several causes including seismic forces, the thrust of arches and vaults, defects of verticality of the panels.

It can usually occur in various forms and mainly for simple overturning (Fig. 1a) as well as for vertical or horizontal flexure (Fig. 1b, c). In the first case, the mechanism consists of the overturning of the wall around a cylindrical hinge on its basis, mainly due to the limited tensile strength of masonry. A typical intervention is realized by means of FRP sheets collocated on the top of the wall and refolded on the orthogonal ones (Fig. 1a).

In the second case, although being well constrained both on the top and on the bottom, the wall can collapse due to out of plane flexural forces which cause the establishment of three hinges, one on the top, one on the bottom and the other in an intermediate position (Fig. 1b). In those cases, usually, FRP sheets with vertical fibers can be collocated on the masonry panel with adequate anchors in order to obtain a “reinforced masonry” in which the compressions are absorbed by masonry while the tensile stresses by the FRP reinforcement.

Finally, the third mechanism can occur when masonry panels well anchored to the lateral walls are not superiorly constrained by the presence of curbs or rigid floors, causing the collapse of a portion of wall as shown in Fig. 1c. Also in these cases, the application of FRP composites on the upper bound of the wall allows enhancing its flexural capacity as in reinforced masonry elements.

Fig. 1 Principal failure mechanisms of masonry walls due to: **a** simple overturning; **b** vertical flexure; **c** horizontal flexure



It has to be noted that when a masonry wall is subjected to an out-of-plane action, the effective response could be considered as intermediate between that above discussed with reference to a rigid body mechanism, or that corresponding to a flexible member.

Several research works were carried out in the past to study the effectiveness of FRP reinforcement on the out-of-plane behaviour of masonry members. Gilstrap and Dolan (1998) provide one of the first overview on the use of FRP reinforcement in masonry members, and examined the state-of-the-art research being conducted for retrofit and repair of these structures. Hamoush et al. (2002) evaluated the influence of externally bonded FRP composites on the out-of-plane shear strength of masonry wall systems by testing eighteen masonry panels under static loading. From obtained results, they concluded that strengthening of unreinforced masonry walls by externally bonded composite overlays

contributes to the flexural performance of the walls, but there appeared to be no significant effect of the reinforcement fiber area on the shear strength of the wall assembly.

From an analytical point of view, Hamed and Rabinovitch (2007) developed a sophisticated analytical model to predict the out-of-plane behavior of FRP reinforced masonry walls. They modeled masonry units and the mortar joints as Timoshenko's beams, while lamination and first-order shear deformation theories were assumed for the FRP strips and the solution was achieved with a complex algorithm. Papanicolaou et al. (2008) tested masonry walls strengthened on both sides with textile-reinforced mortars or with FRP under out-of-plane cyclic loading. Additional comparisons were also made with respect to Near Surface Mounted (NSM) reinforcement. They investigated on the effect of mortar-based and resin-based matrix materials, the number of layers, the orientation of the moment vector with respect to the bed joints and the performance of textile reinforced mortar (TRM) or FRP jackets in comparison to NSM strips. It was concluded that TRM jacketing provides substantial increase in strength and deformability. Hamed and Rabinovitch (2010) refined their previous work by a combined experimental-theoretical characterization of the behavior of the FRP strengthened walls. In particular, they investigated on the behaviour of realistically supported strengthened walls under conditions that restrict the elongation and allow the development of the arching action. More recently, Gattesco and Boem (2014, 2015) presented the results of a numerical investigation on the out-of-plane bending behaviour of cobblestone masonry walls. Researchers carried out numerical simulations utilising a two-dimensional nonlinear model, and evaluated the efficiency of GFRP reinforced mortar coatings.

Within this framework, in the present paper a simplified numerical-analytical approach for the assessment of the flexural behaviour of out-of-plane loaded masonry walls is presented. The model is based on a simplified representation of the member, the latter modeled as a cantilever beam. Mechanical non-linearity is introduced by means of moment–curvature relationships, deduced with proper constitutive laws of masonry and by taking into account the ultimate debonding strain of FRP. Second order effects are considered by adopting an iterative step-by-step procedure. Comparisons are made in terms of moment–curvature and load–displacement curves with experimental data available in the literature and with non-linear finite element analyses, showing both good agreement. Finally, parametric considerations on the reinforcement percentages are made in terms of strength and ductility.

1.1 Analytical investigation

A numerical/analytical model was developed able to predict the lateral load–deflection curves of out-of-plane loaded masonry walls. The model was based on a continuum discretization of the wall, considered as a uniaxial member (beam) and loaded with a generic load profile.

Preliminarily, constitutive law of masonry in compression was calibrated based on some experimental data available in the literature, and adopted for the sectional analysis.

1.1.1 Constitutive laws of constituent materials

The compressive behaviour of calcarenite masonry was modeled by means of the axial stress–strain law proposed by Sargin (1971) and modified by Cavaleri et al. (2005).

$$\tilde{\sigma} = \frac{A \cdot \tilde{\epsilon} + (D - 1) \cdot \tilde{\epsilon}^2}{1 + (A - 2) \cdot \tilde{\epsilon} + D \cdot \tilde{\epsilon}^2} \tag{1}$$

where σ_0 and ϵ_0 were the peak stress and strain respectively, and ultimate compressive strain was assumed as $\epsilon_u = 2\epsilon_0$.

The parameters A and D defined the shape of the curve. In particular, the value imposed to A could be considered as the ratio between the tangent and the secant modulus, while D regulated the shape of the descending branch. More in detail, the higher D the more horizontal will be the trend of the post-peak response. Conversely, a brittle behaviour was associated to low values of D—i.e. the slope of the softening branch increases. As an example, Fig. 2 plots the constitutive law expressed by Eq. (1). Values shown in Fig. 2 refer to the experimental data of Accardi et al.(2007a), that are adopted in the following sections for numerical applications.

The tensile behaviour of FRP was modelled with a classic linear relationship, being the tensile strength of the composite defined in the following form

$$f_t = E_f \cdot \epsilon_{fu} \tag{2}$$

where E_f and ϵ_{fu} are the elastic modulus and ultimate strain of FRP respectively.

It should be noted that particular care has to be addressed on the evaluation of the ultimate strain. This last should be defined not only with reference to the ultimate tensile stress but mainly referring to the ultimate debonding strain ϵ_{du} . This value could be expressed as a function of the fracture energy G_f , as proposed by Täljsten (1996), and the ultimate pull-out load could be expressed by

$$F_u = b_f \sqrt{\frac{2 \cdot E_f \cdot t_f \cdot G_f}{1 + \alpha}} \tag{3}$$

where b_f and t_f were the width and the thickness of the FRP strip respectively, while α was the axial stiffness ratio between the two adjacent materials

$$\alpha = \frac{E_f \cdot A_f}{E \cdot A} \tag{4}$$

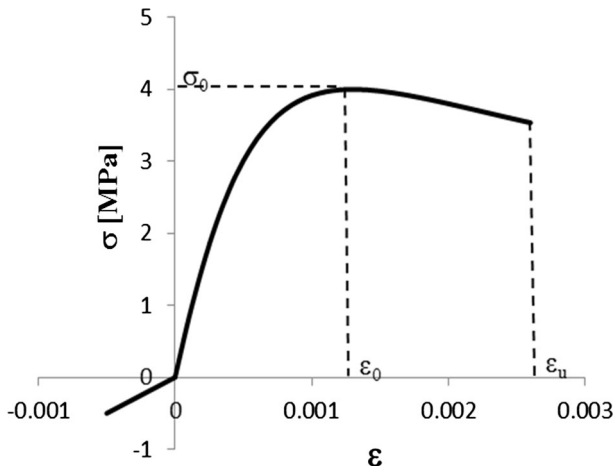


Fig. 2 Stress-strain model of Sargin (1971) adapted for masonry

being A_f the nominal area of the FRP strip, E the Young modulus of the material bonded to the composite and A the area of the transverse section of the member.

The evaluation of fracture energy is a quite difficult task, especially for actual applications and particularly for existing structural members. For this reason, several technical codes provided formulations able to relate the fracture energy to the mechanical properties of the base material—i.e. American code ACI 440/2010, international instructions FIB 2001 for concrete, Italian guidelines CNR-DT 200/2013 for masonry. As an example, the fracture energy could be determined experimentally, by expressing G_f from Eq. (3) and neglecting the value of α

$$G_f = \frac{F_u^2}{2 \cdot b_f^2 \cdot E_f \cdot t_f} \tag{5}$$

and F_u is measured experimentally.

Equation (5) allowed evaluating the fracture energy experimentally, and expressing this as a function of the mechanical properties of the base material. As an example, Accardi et al. (2007a) expressed the fracture energy as a function of the compressive strength for calcarenite stone masonry, finding an analytical expression, which fits the experimental values obtained by pull-out tests

$$G_f = 0.06 \sqrt{f_b} \tag{6}$$

Figure 3 shows the trend of Eq. (6) and related experimental data obtained in Accardi et al. (2007a). Substituting Eq. (6) in Eq. (3) the following expression of the ultimate debonding load hold

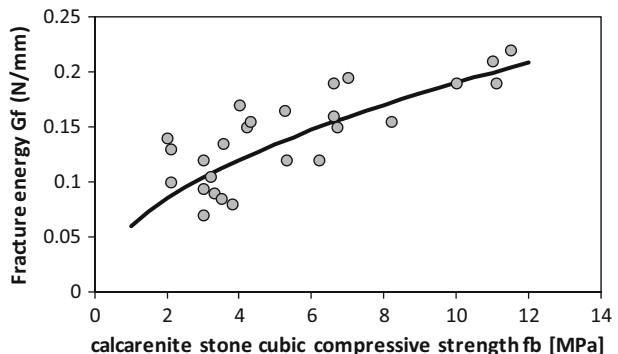
$$F_u = b_f \sqrt{0.12 \cdot E_f \cdot t_f \cdot \sqrt{f_b}} \tag{7}$$

Finally, the ultimate debonding strain of FRP was obtained as

$$\epsilon_{du} = \frac{F_u}{E_f \cdot A_f} = \sqrt{\frac{0.12 \cdot \sqrt{f_b}}{t_f \cdot E_f}} \tag{8}$$

The resultant constitutive law of FRP in tension was defined by a linear stress–strain relationship shown in Fig. 4. Also in this case, values refer to the experimental

Fig. 3 Experimental correlation between fracture energy and compressive strength $G_f - f_b$ Accardi et al. 2007a



investigation of Accardi et al. (2007a). It is worth to note that the debonding strain value is substantially lower than ultimate tensile strain at failure.

1.1.2 Sectional analysis

The sectional analysis of the masonry wall was undertaken with the target of calculating proper moment–curvature curves. Calculation was made with reference to rectangular sections under the assumptions of plane sections until failure, perfect bond between masonry and FRP, and masonry with proper compressive and tensile stress–strain relationships (discussed above).

The definition of moment–curvature curves was achieved by direct integration of equilibrium equations, the latter related to sections with uniaxial bending moment and an axial load (Fig. 5), the latter to be considered constant.

If the hypothesis of full reacting section and referring to symbols reported in Fig. 5, meaning maximum tensile strain less than peak, equilibrium equations could be written in the following form

$$R - F_t - T = N \tag{9}$$

$$R \left[c + \left(t + \frac{t_f}{2} - x_c \right) \right] + T \left[d - \left(t + \frac{t_f}{2} - x_c \right) \right] = M + N \left(\frac{t}{2} + \frac{t_f}{2} \right) \tag{10}$$

where R and T are the resultant forces of internal compressive and tensile stresses in the masonry section, while F_t is the tensile force in the FRP strip and N is the external axial force.

As it is well-known, Eqs. (9, 10) could be expressed as a function of the unknown curvature and by expressing explicitly the internal forces of the section

$$\int_0^{\epsilon_c} \frac{b}{\phi} \cdot \sigma(\epsilon) \cdot d\epsilon - A_f \cdot E_f \cdot \epsilon_{du} - \int_0^{(\phi \cdot t - \epsilon_c)} \frac{E_t \cdot b \cdot \epsilon}{\phi} \cdot d\epsilon = N \tag{11}$$

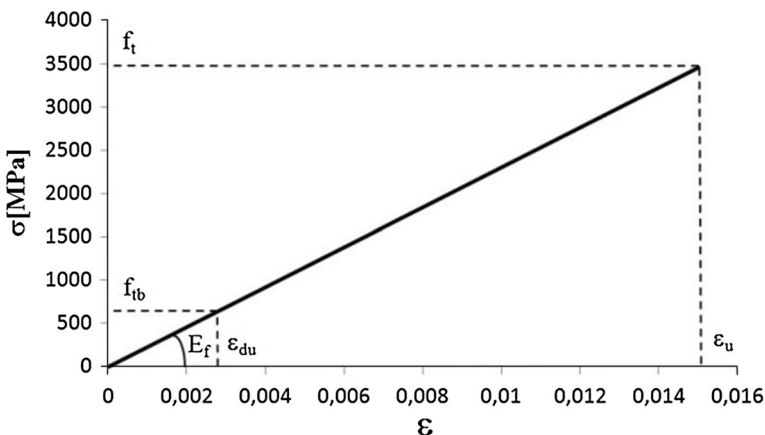


Fig. 4 Stress–strain relationship for FRP in tension

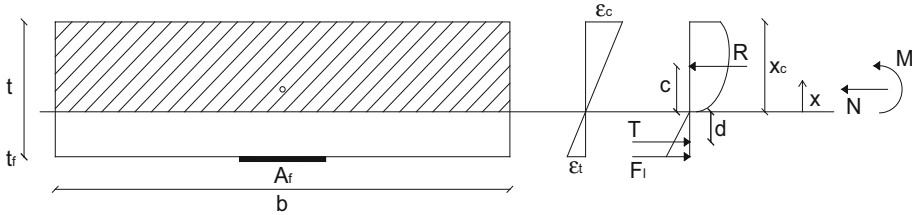


Fig. 5 Transverse cross section of the wall with strain and stress distribution

$$\int_0^{\varepsilon_c} \frac{b}{\varphi^2} \cdot \sigma(\varepsilon) \cdot \left[\varepsilon + \left(t + \frac{t_f}{2} - \frac{\varepsilon_c}{\varphi} \right) \right] \cdot d\varepsilon + \int_0^{(\varphi \cdot t - \varepsilon_c)} \frac{E_t \cdot b \cdot \varepsilon^2}{\varphi^2} \cdot \left[\varepsilon - \left(t + \frac{t_f}{2} - \frac{\varepsilon_c}{\varphi} \right) \right] \cdot d\varepsilon = M + N \left(\frac{t}{2} + \frac{t_f}{2} \right) \tag{12}$$

with $\varepsilon_t < \varepsilon_{ct}$ and $\varepsilon_{ct} = \frac{\sigma_t}{E_t}$.

Differently, when $\varepsilon_t > \varepsilon_{ct}$, equilibrium equations of the section were written as

$$\int_0^{\varepsilon_c} \frac{b}{\varphi} \cdot \sigma(\varepsilon) \cdot d\varepsilon - A_{FRP} \cdot E_f \cdot \varepsilon_{du} - \int_0^{\varepsilon_{ct}} \frac{E_t \cdot b \cdot \varepsilon}{\varphi} \cdot d\varepsilon = N \tag{13}$$

$$\int_0^{\varepsilon_c} \frac{b}{\varphi^2} \cdot \sigma(\varepsilon) \cdot \left[\varepsilon + \left(t + \frac{t_f}{2} - \frac{\varepsilon_c}{\varphi} \right) \right] \cdot d\varepsilon + \int_0^{\varepsilon_{ct}} \frac{E_t \cdot b \cdot \varepsilon^2}{\varphi^2} \cdot \left[\varepsilon - \left(t + \frac{t_f}{2} - \frac{\varepsilon_c}{\varphi} \right) \right] \cdot d\varepsilon = M + N \left(\frac{t}{2} + \frac{t_f}{2} \right) \tag{14}$$

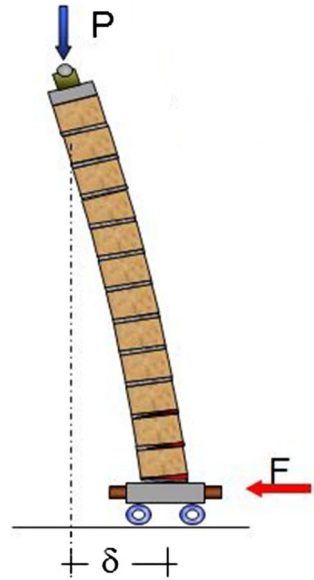
Equations (11–14) allowed calculating the values of curvature φ and the corresponding moment M for known geometry of the section and for a fixed value of ε_c . The procedure was repeated until reaching the ultimate value of masonry compressive strain or the debonding strain in the FRP strip.

Comparisons were made between the experimental data of Accardi et al. (2007b) (Fig. 6) and the analytical predictions made with the above described procedure.

Experimental data refers to masonry walls having thickness of 210 mm, width equal to 740 mm and height of 2100 mm. In particular, masonry constituting the panels was made by calcarenite blocks with sizes 360 × 210 × 160 mm and mortar joints with thickness equal to 10 mm. The unreinforced URM specimen referred to unreinforced control specimen, while FRP-W4 referred to a panel reinforced with four CFRP strips having width of 50 mm and thickness of 0.13 mm. Panels were tested under flexure with a constant axial load of 80 kN.

Regarding the analytical assumptions, the above described constitutive law were adopted. The test results obtained in Accardi et al. (2007a) were considered to choose compressive strength, peak strain and to calibrate the above mentioned A and D parameters of the compressive stress–strain relationship. In particular, Accardi et al. (2007b) performed monotonic compressive tests on calcarenite masonry samples with three unit courses and normal-grade mortar layers with thickness equal to 10 mm. Average peak stress was $\sigma_0 = 4$ MPa, peak strain $\varepsilon_0 = 1.3$ mm/m, while from best fitting of experimental curves the deduced shape parameters were $D = 1.5$ and $A = 2.8$. Finally, the uniaxial constitutive law of calcarenite masonry was completed by assuming a linear

Fig. 6 Test set-up adopted in Accardi et al.(2007b)



stress–strain relationship for masonry in tension, by assuming also tensile strength $\sigma_t = 0.35$ MPa and elastic modulus $E_t = E_c/2 = 2000$ MPa.

Considering the FRP strip, data provided by the producer considered the tensile strength equal to 3450 MPa, ultimate strain $\varepsilon_{fu} = 1.5\%$, which corresponded to a Young modulus equal to $E_f = 230,000$ MPa. Epoxy resin was adopted to apply the reinforcement; properties declared by the producer were tensile strength equal to 30 MPa.

With reference to the calculation of debonding stress and strain, the latter was assumed equal to $\varepsilon_{du} = 2.71$ mm/m, having set $f_b = 3.37$ MPa as discussed in Accardi et al. (2007a), and finally the debonding tensile stress of FRP was calculated as $f_{tb} = E_f \cdot \varepsilon_{du} = 624.29$ MPa.

As it could be observed from Fig. 7, the analysis provided a little overestimation of the stiffness in both cases. This fact was probably due to the flexibility of the base restraint, which cannot be included in the sectional analysis. First cracking and ultimate moment were quite well predicted for the URM wall while an underestimation hold for FRP reinforced specimen.

1.1.3 Proposed model

After defining the sectional response in terms of moment–curvature diagram, a numerical-analytical procedure was adopted able to find the overall flexural behaviour of the wall in terms of lateral force F versus lateral displacement δ curves.

The main hypothesis was related to the beam approximation of the wall. This consideration should be considered valid when the lateral joints of studied panel with walls in orthogonal direction are poor or when the studied panel has a great value of the width-to-height ratio. This means that lateral constraints are far enough such that a middle strip of the wall with unit width can be studied to represent the flexural behaviour of the central part of the member.

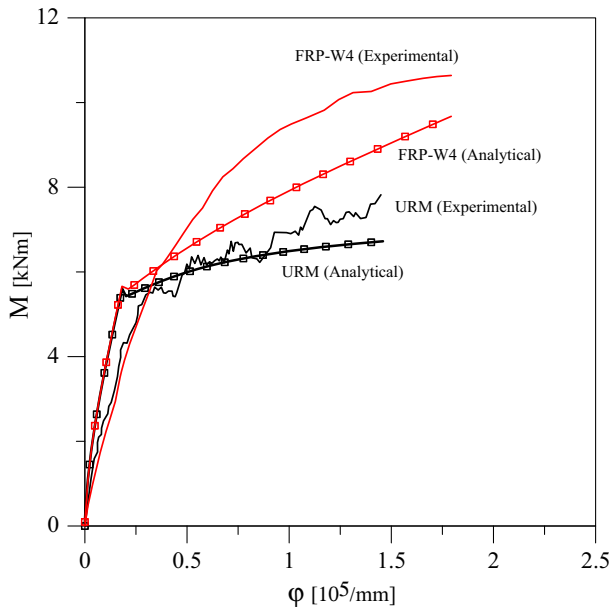


Fig. 7 Comparison between experimental and analytical moment–curvature curves (Experimental data of Accardi et al. 2007a)

With these assumptions, the panel is here represented by a cantilever beam, loaded with an horizontal force F_j , an axial force P and a bending moment M_j at the top (Fig. 8a). The lateral force F_j represents the out-of-plane seismic load, the axial load P idealizes the effect of the gravity loads, while the bending moment M_j is related to the possibility that a restraining condition should be provided in the panel (e.g. a wall with restrained rotation at the ends). As it is well-known, for a general calculation including second order effects, F_j , P and M_j should be unknown, each depending on the actual value of the lateral displacement. However, aiming to propose a simplified model for easy parametric calculations and according to experimental results (Accardi et al. 2007a) the following assumptions are made: the axial force P is considered constant during the loading process; the bending moment at the top M_j is assumed as a function of the lateral force F_j . On the basis of this last assumption, M_j is evaluated as $M_j = F_j \zeta L$, where ζ is a coefficient depending on the effective restraining level at the top. In particular, the product ζL defines the distance between the top of the member and the section with zero internal bending moment according to first order theory (e.g. $\zeta = 0$ for cantilever beam, $\zeta = 0.5$ for beam with fixed rotation at both ends).

The cantilever beam is subdivided in n parts with equal length Δ (Fig. 8a), and a control point coincident with each middle section is defined. Defining the coordinate vector of each control point as

$$\underline{x} = \begin{bmatrix} x_1 \\ \vdots \\ x_n \end{bmatrix} \quad (15)$$

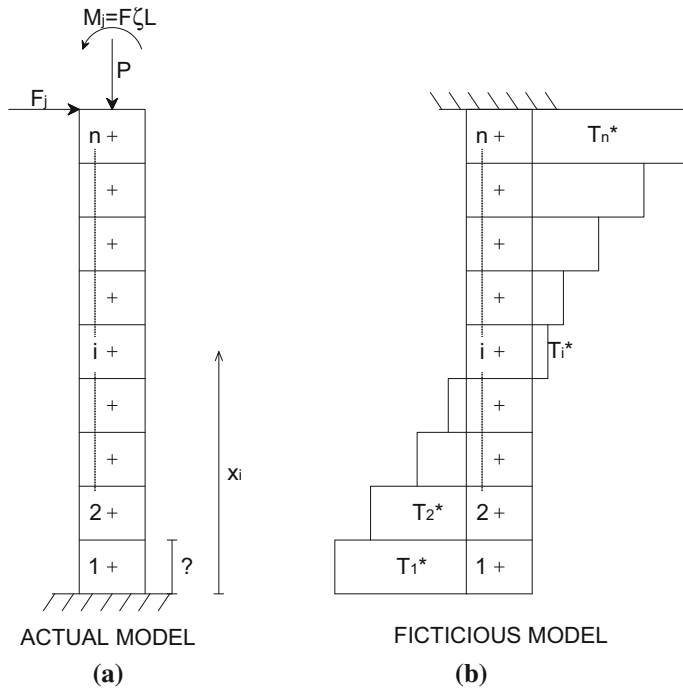


Fig. 8 Model for calculation of the flexural response; **a** geometry and load path; **b** Mohr’s scheme for displacement calculation

the first order moment in each point is defined by the vector

$$\underline{M_I} = \begin{bmatrix} M_{I,1} \\ \vdots \\ M_{I,n} \end{bmatrix} = F_j L (\zeta - 1) + F_j \underline{x} \tag{16}$$

while the second order moment is calculated as

$$\underline{M_{II}} = \begin{bmatrix} M_{II,1} \\ \vdots \\ M_{II,n} \end{bmatrix} = -P(w_n - \underline{w}) \tag{17}$$

being w_n the top displacement of the beam and \underline{w} the vector of displacements in each control point. The total bending moment is obviously calculated as the sum of Eqs. (16) and (17) in the form

$$\underline{M} = \begin{bmatrix} M_I \\ \vdots \\ M_n \end{bmatrix} = \underline{M_I} + \underline{M_{II}} = F_j L (\zeta - 1) + F_j \underline{x} - P(w_n - \underline{w}) \tag{18}$$

After knowing the bending moment, the effective displacement can be calculated by adopting the Mohr’s analogy (Fig. 8b) and assuming the curvature as constant in each beam’s piece. In the Mohr’s model, the fictitious force on each portion is calculated as

$$\underline{T}^* = \begin{bmatrix} T_1^* \\ \vdots \\ T_n^* \end{bmatrix} = \underline{\Phi} \cdot \Delta \tag{19}$$

being $\underline{\Phi}$ the vector of curvatures in each control point, defined as a function of the bending moment expressed by Eq. (18)

$$\underline{\Phi} = \begin{bmatrix} \phi_1(M_1) \\ \vdots \\ \phi_n(M_n) \end{bmatrix} \tag{20}$$

On the basis of the patch shown in Fig. 8b, the displacement of the i -th control point is finally obtained in the form

$$w_i = - \sum_{k=1}^i T_k^*(x_i - x_k) \tag{21}$$

that can be generalised for each control point by the following expression

$$\underline{w} = \begin{bmatrix} w_1 \\ \vdots \\ w_n \end{bmatrix} = - \begin{bmatrix} 0 & 0 & 0 & 0 & 0 \\ x_2 - x_1 & 0 & 0 & 0 & 0 \\ \vdots & \vdots & 0 & 0 & 0 \\ x_i - x_1 & x_i - x_2 & x_i - x_{i-1} & 0 & 0 \\ x_n - x_1 & x_n - x_2 & \dots & x_n - x_{n-1} & 0 \end{bmatrix} \cdot \begin{bmatrix} T_1^* \\ \vdots \\ T_n^* \end{bmatrix} = -\underline{D} \cdot \underline{T}^* \tag{22}$$

The n -th equation provided by the system (22) allows calculating the top displacement in the form

$$w_n = -\underline{T}^*(x_n - \underline{x}) \tag{23}$$

The solution can be achieved with an iterative procedure. The geometrical features are assigned and the axial load P is assumed to be known and constant during the analysis. The moment–curvature diagram is preliminary calculated by means of the procedure described in the previous section for assumed axial load P . (1) A value is assigned to the lateral force F_j at the j -th step; (2) the first order moments are calculated by Eq. (16) and second order moments are assumed to be zero at the first iteration ($\underline{M}_{II}^{(1)} = \underline{0}$); (3) the corresponding curvature vector $\underline{\Phi}^{(1)}$ can be evaluated by means of Eq. (20), and fictitious loads $\underline{T}^{*(1)}$ by means of Eq. (19); (4) lateral displacements at first iteration $\underline{w}^{(1)}$ are therefore calculated with Eq. (22); (5) obtained displacements $\underline{w}^{(1)}$ are subsequently adopted to evaluate second order moments at the successive iteration $\underline{M}_{II}^{(2)} = -P(w_n^{(1)} - \underline{w}^{(1)})$; (6) the updated value of total moment is calculated as $\underline{M}^{(2)} = \underline{M}_I + \underline{M}_{II}^{(2)}$ and points (3) and (4) are repeated, calculating the new values of lateral displacements $\underline{w}^{(2)}$. The final values are obtained when the balanced difference between the deflection at the $k + 1$ -th and k -th iteration was less than a fixed tolerance $\frac{w_n^{k+1} - w_n^k}{w_n^k} < 0.01$.

In this way a value of displacement at each control point was calculated for a fixed lateral force F_j . The overall force–displacement curve was therefore obtained by assigning a new value to the lateral force F_{j+1} and repeating the above mentioned procedure.

Figure 9 shows the results given by the application of the above mentioned procedure for an out-of-plane loaded masonry panel with the same data described in the previous section, referring to the experimental work of Accardi et al. (2007b). In particular, the lateral load–deflection curves have shown that increases of ultimate lateral force and deflection were expected with an increase of the reinforcement ratio. Second order effects were neglected in order to stress the achievable increase of lateral load capacity. As it was expected, the theoretical effect of adding external CFRP strips did not affect the initial stiffness, but it should enhance strength and ductility. The response of the unreinforced wall was characterized only by a non-linear branch with an ascending trend until brittle failure. Conversely, the effect of adding external flexural reinforcement gave to the curves a second ascending branch with a reduced slope, which means that the walls continued to sustain the external load also after cracking.

It should be noted that for each case, failure was reached due to compressive crushing of masonry.

1.2 Numerical and experimental validation

A numerical investigation was also performed to validate the results obtained with the proposed model.

The finite element method (FEM) was adopted to model the behaviour of panels, as shown in La Mendola et al. (2009), by using the code LUSAS Release. Plane stress elements QPM8 were considered to model blocks and mortar (Fig. 10). These were regular quadrilateral elements with eight nodes, using quadratic integration and the Gauss 3×3 numerical scheme. Both block units and mortar elements were characterized by a linear constitutive law.

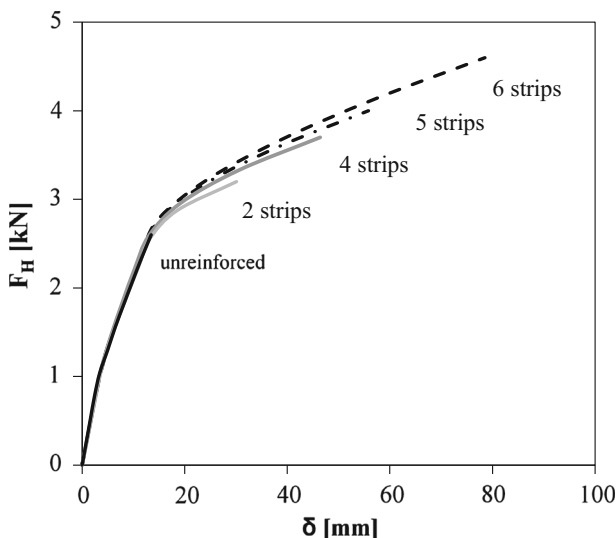
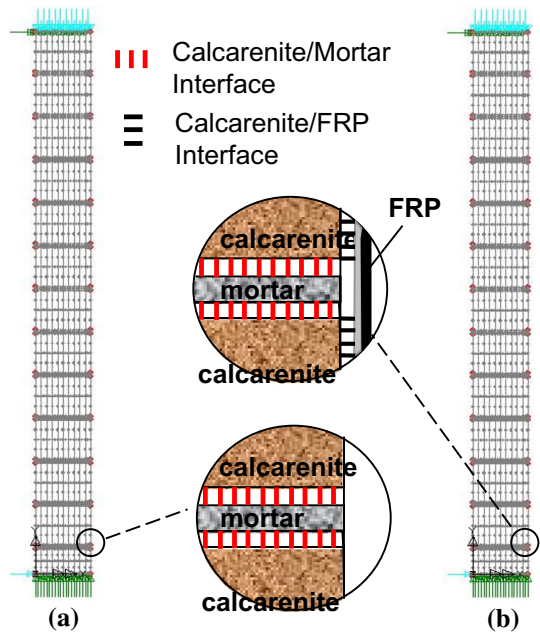


Fig. 9 Analytical lateral force–deflection curves: effect of the reinforcement amount

Fig. 10 Numerical model in LUSAS



It should be noted that linear constitutive laws were considered since the non-linearity of the overall behaviour was given by the connections by interface elements. This assumption allows to reduce the computational effort. The connection between the block and the mortar layer was achieved by means of IPN6 elements. This was a six node interface element between two lines, having no thickness and quadratic interpolation. This element proved to be suitable to model interlayer failure and crack propagation. Contact zones were considered block-mortar and FRP-masonry and modelled with a bi-linear interface law. Interface elements were characterized by a damage model for delamination, allowing the failure mode for opening and/or sliding. The interface model required three parameters: initial failure strength f_{\max} , corresponding opening u_o and fracture energy G_f . The ratio between the initial failure strength, f_{\max} , and the limit displacement u_o gives the interface elastic stiffness k^I . Several analyses were carried out for calibrating interface parameters. In particular, URM specimens were modeled and the values assumed for f_{\max} , k^I and G_f were changed until good accordance was recorded between the experimental and numerical lateral load versus deflection curves. Finally, the following parameters were assumed $f_{\max} = 0.055 \text{ N/mm}^2$; $k^I = 34.78 \text{ N/mm}^3$, $G_f = 0.0025 \text{ N/mm}$, which were also adopted for FRP reinforced walls.

The model included geometric non-linearity on the basis of 2nd order theory. Equilibrium conditions were created in nodes of the calculation model, considering the deformed shape. Stiffness matrix was updated for each load step of iteration and equilibrium equations are solved by the Arc-length method.

Displacement-controlled static analysis were performed by imposing a deflection of 0.5 mm/step. Reaction force was measured by means of monitoring points placed at joints of the base constraint.

Figure 11 shows the comparisons between the results obtained theoretically and the experimental data. Analytical and numerical predictions were plotted together with

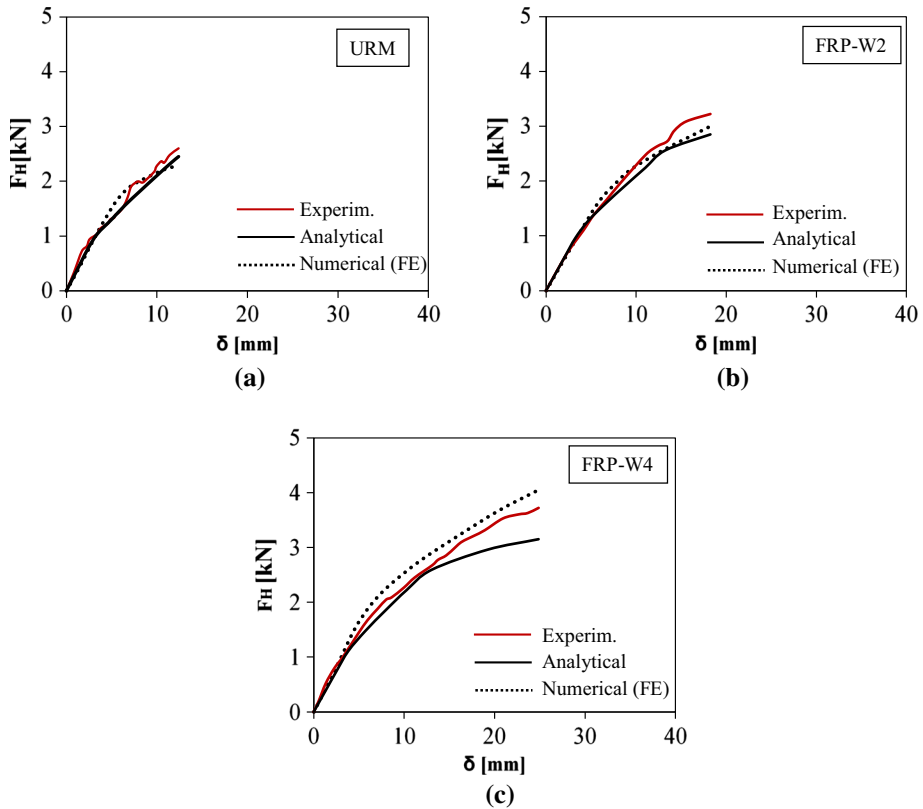


Fig. 11 Comparison between experimental data and theoretical results (experimental data of Accardi et al. (2007a))

experimental results. A good accordance could be observed between the three curves, showing as the proposed model could represent a simplified assessment tool for preliminary evaluation of a strengthening design. Particularly, strength and stiffness were better predicted by the proposed model for URM specimen (Fig. 11a).

Good predictions were also obtained for reinforced specimens; the analytical prediction was in good accordance with the FE analysis for FRP-W2 specimen with a little underestimation of the overall response—i.e. difference of about 12% for the peak load.

The theoretical prediction provided by the proposed model was also in good agreement with the experimental curve of specimen FRP-W4. A slight underestimation of about 13% of peak load was calculated, while the FE analysis provided a little overestimation of about 12%.

1.3 Parametric analysis

The adopted sectional analysis allowed to make some considerations about designing strengthening techniques by means of FRP reinforcement.

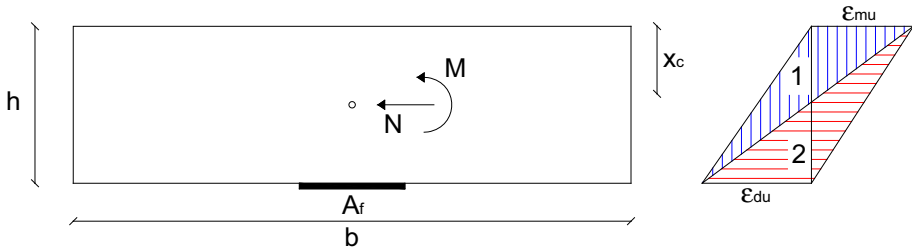


Fig. 12 Transverse section and possible strain profiles at failure

Figure 12 shows the patch of the cross section of the wall together with a range of possible strain profiles at failure. Reinforcement in the compression zone was neglected due to the fact that FRP was considered reacting only in tension.

It was clear that failure could be addressed to FRP delamination or to masonry compressive crushing. In the first case, delamination was achieved when debonding strain ϵ_{du} was reached on the FRP-masonry fiber (range 1), while in the second case failure of masonry occurred due to the reaching of maximum compressive strain of masonry ϵ_{mu} (range 2). The ultimate curvature increased with the increase of the neutral axis depth among range 1, and differently it decreased for range 2. As a consequence, the greater value of ultimate curvature was obtained in correspondence of balanced failure, meaning theoretical contemporary failure of masonry and FRP. In this way, balanced failure could be considered as an optimal configuration for design purposes, due it allowed obtaining the greater ductility of the wall.

The first equilibrium equation of the section at failure could be expressed in the following normalised form

$$\frac{S_1(\epsilon_{mu})}{\varphi_u \cdot h} - \gamma_f \cdot \omega_f = n \tag{24}$$

where

$$\int_0^{\epsilon_{mu}} \frac{\sigma(\epsilon)}{f_b} \cdot d\epsilon = S_1(\epsilon_{mu})$$

$$n = \frac{N}{b \cdot h \cdot f_b}, \quad \omega_f = \frac{A_f \cdot f_{tb}}{b \cdot h \cdot f_b} \quad \text{and} \quad \gamma_f = \frac{\sigma_f}{f_{tb}}$$

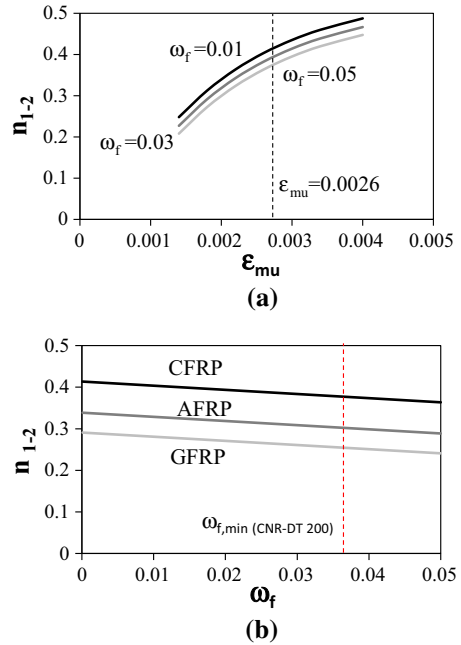
Equation (15) should be particularized for range 1 considering $\gamma_f = 1$. With the same assumptions of symbols, the equilibrium equation could be specified for balanced failure

$$\frac{S_1(\epsilon_{mu})}{\varphi_{u1-2} \cdot h} - \omega_f = n_{1-2} \tag{25}$$

Equation (25) proved that the normalised axial force n_{1-2} corresponding to the change from debonding to crushing failure depended by the ultimate compressive failure of masonry ϵ_{mu} and by the mechanical ratio of FRP reinforcement ω_f .

Figure 13a shows the trend of n_{1-2} as a function of the ϵ_{mu} and for three different values of ω_f . Results are reported for three different kinds of composite, namely Carbon, Aramid and Glass FRP. Moreover, the value of ultimate strain 0.0026 adopted for the previously discussed analyses was highlighted. It could be observed that n_{1-2} mainly depended by

Fig. 13 Variation of the normalised balanced axial load **a** as a function of the ultimate compressive strain of masonry; **b** as a function of the mechanical ratio of FRP

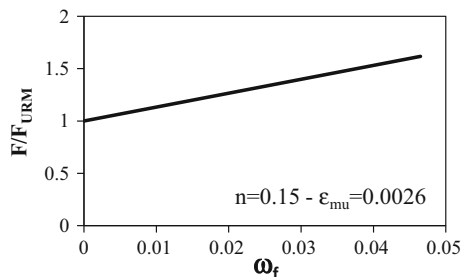


ultimate compressive strain of masonry, increasing for higher values of ϵ_{mu} . This fact reflected the theoretically expected evidence that flexural ductility increased when the base material have a more extended post-peak branch. Furthermore, it could be noted that the balanced failure axial load decreased with an increase of the amount of FRP ratio (Fig. 13b).

A reasonable design procedure should be related not only to a prescribed value of FRP amount for strength purposes, but also ensuring the higher value of ultimate curvature. In this manner, an amount of FRP could be chosen by means of Fig. 13a, by selecting the ultimate compressive strain of existing masonry and imposing $n_{1-2} = n_d$, where n_d is the design normalised axial load. Finally, the ultimate lateral load should be checked for the selected reinforcement ratio.

Figure 14 shows the enhancement of ultimate lateral force with the increase of FRP mechanical ratio and for the fixed parameters adopted for above presented analyses ($n = 0.15$, $\epsilon_{mu} = 0.0026$). In this way the strength increase could be checked and compared with lateral force demand imposed by code requirements.

Fig. 14 Increase of ultimate flexural lateral load as a function of FRP reinforcement ratio



2 Conclusions

This paper presented a theoretical analysis about the flexural behaviour of out-of-plane loaded masonry walls reinforced with FRP strips. A simple model was proposed, based on a sectional analysis which included the effective non-linear constitutive law of masonry in compression, the tensile strength of masonry, and the effect of debonding at masonry-FRP interface. A fiber model allowed to reproduce easily test configurations of masonry walls with a lateral force. Second order effects were also included by means of an iterative procedure. Results obtained by the proposed model were compared with experimental data available in the literature and with numerical FE simulations. From obtained results the following conclusions could be drawn:

- the inclusion of second order effects and ultimate debonding strain is crucial to obtain a realistic response of the wall;
- failure could occur due to crushing of masonry or debonding of FRP. An optimal design configuration should be addressed to the contemporary achievement of both mechanisms;
- the normalised axial force corresponding to the balanced failure proved to be a function of the ultimate compressive strain of masonry and of the mechanical ratio of FRP.

References

- Accardi M, Cucchiara C, Failla A, La Mendola L (2007a) CFRP flexural strengthening of masonry walls: experimental and analytical approach. In: FRPRCS-8, Patras, Greece
- Accardi M, Cucchiara C, Failla A, La Mendola L (2007b) Strengthening of masonry walls subjected to out-of-plane loads using CFRPs. In: Atti del Workshop Materiali ed Applicazioni Innovativi per il Progetto in Zona Sismica e la Mitigazione della Vulnerabilità delle Strutture, Fisciano, 12–13 Febbraio, pp 231–238
- ACI Committee 440 (2010) Guide for the design and construction of externally bonded FRP systems for strengthening concrete structures
- Cavaleri L, Failla A, La Mendola L, Papia M (2005) Experimental and analytical response of masonry elements under eccentric vertical loads. *Eng Struct* 27(8):1175–1184
- CNR-DT 200 R1/2013 (2013) Istruzioni per la Progettazione, l'Esecuzione ed il Controllo di Interventi di Consolidamento Statico mediante l'utilizzo di Compositi Fibrorinforzati
- FIB Bulletin no.14 (2001) Externally bonded FRP reinforcement for RC structures, p 138
- FIB Bulletin no. 40 (2007) FRP reinforcement in RC structures, p 160. ISBN: 978-2-88394-080-2
- Gattesco N, Boem I (2014) Out-of-plane behaviour of masonry walls strengthened with a GFRP reinforced mortar coating. In: Proceedings of the 9th international masonry conference, 7–9 lug. 2014, Guimaraes, Portugal
- Gattesco N, Boem I (2015) Numerical simulation of the out-of-plane performance of masonry walls strengthened with a GFRP reinforced mortar. In: Proceedings of the 15th international conference on civil, structural and environmental engineering computing, CC2015, paper 78, 1–4 Sept 2015, Prague, Czech Republic
- Gilstrap JM, Dolan CW (1998) Out-of-plane bending of FRP-reinforced masonry walls. *Compos Sci Technol* 58:1277–1284
- Hamed E, Rabinovitch O (2007) Out-of-plane behavior of unreinforced masonry walls strengthened with FRP strips. *Compos Sci Technol* 67:489–500
- Hamed E, Rabinovitch O (2010) Failure characteristics of FRP-strengthened masonry walls under out-of-plane loads. *Eng Struct* 32:2134–2145
- Hamoush S, McGinley M, Mlakar P, Terro MJ (2002) Out-of-plane behavior of surface-reinforced masonry walls. *Constr Build Mater* 16:341–351
- ISIS Design Manual No. 4 (2008) FRP rehabilitation of reinforced concrete structures. ISIS Canada Corporation

- La Mendola L, Amato G, Licata V, Accardi M (2009) Numerical analysis and experimental comparison on CFRP reinforced masonry walls subjected to transverse loads. In: Protection of historical buildings, PROHITECH 09
- LUSAS. Modeller reference manual, FEA Ltd., Kingston-upon-Thames, UK
- Papanicolaou CG, Triantafillou TC, Papathanasiou M, Karlos K (2008) Textile reinforced mortar (TRM) versus FRP as strengthening material of URM walls: out-of-plane cyclic loading. *Mater Struct* 41:143–157
- Sargin M (1971) Stress–strain relationship for concrete and the analysis of structural concrete sections, study 4. In: Solid Mechanics Division; University of Waterloo, Waterloo, Canada
- Täljsten B (1996) Strengthening of concrete prisms using the plate-bonding technique. *Int J Fract* 82:253–266